geosciences

MDPI

Article

Petrology of Lancang (Upper Mekong) River Sand

Daxin Fang [1,2], Xiumian Hu [1,*], Eduardo Garzanti [3], Wen Lai [4] and Fengting Chen [1]

[1] School of Earth Sciences and Engineering, Nanjing University, Nanjing 210023, China; dxfang@itpcas.ac.cn (D.F.); fengtingchen@smail.nju.edu.cn (F.C.)
[2] State Key Laboratory of Tibetan Plateau System, Environment and Resources (TPESER), Institute of Tibetan Plateau Research, Chinese Academy of Sciences, Beijing 100101, China
[3] Department of Earth and Environmental Sciences, University of Milano-Bicocca, 20126 Milan, Italy; eduardo.garzanti@unimib.it
[4] School of Geography and Environmental Engineering, Gannan Normal University, Ganzhou 341000, China; laiwen@gnnu.edu.cn
* Correspondence: huxm@nju.edu.cn

Abstract

The texture and composition of river sediments are key to understanding the characteristics of source rocks, chemical weathering in the source area, physical modifications during transport, and human impacts within watersheds. This study analyzes 47 very fine to coarse size sands from the Lancang (Upper Mekong) River in China to monitor compositional variations and assesses the contribution of different geological units to trunk-river sediments. Lancang River sands are mostly feldspatho-quartzo-lithic in composition, with quartz content increasing downstream at the expense of lithic fragments (especially of carbonate lithics). Sand is mostly generated from the Lincang and Baoshan blocks, with subordinate contributions from the Simao and Changdu blocks. This study provides new insights into erosional and depositional processes in the Lancang River and emphasizes the impact of human activities on river sediment transport.

Keywords: Lancang River; sand petrography; provenance analysis; anthropogenic impact

Academic Editor: Eun Young Lee

Received: 15 July 2025
Revised: 26 October 2025
Accepted: 28 October 2025
Published: 31 October 2025

Citation: Fang, D.; Hu, X.; Garzanti, E.; Lai, W.; Chen, F. Petrology of Lancang (Upper Mekong) River Sand. *Geosciences* **2025**, *15*, 415. https://doi.org/10.3390/geosciences15110415

1. Introduction

River sediments can be used to trace erosion patterns across source areas and short-term to long-term watershed evolution under the impact of tectonics, climate, and human activities [1–4]. By analyzing modern river sediments, we can examine physical and chemical processes within well-constrained geological, geomorphological, and climatic settings, helping us to better understand how sediments are generated, transported, and ultimately deposited [5].

The surface uplift of the Himalayan Mountains and Tibetan Plateau resulted from the continuing collision between the Indian and Asian plates [6,7] and initiated the formation of large Asian rivers, including the Mekong. The Lancang headwaters of the Mekong River contribute ~50% of the total sediment supplied annually to the South China Sea, amounting to 160 million tons [8,9]. Located in a tectonically active cold–humid climatic zone, the Lancang catchment presents excellent conditions for studying sediment provenance and recycling [10,11]. Previous geochronological and geochemical studies of Lancang River sediments revealed predominantly felsic source rocks exposed in the Northern Qiangtang and Yidun blocks [12,13], but without adequate consideration of sediment recycling and quantitative assessment of sediment contribution from different geological units.

This study analyzes the textural and compositional characteristics of river sands and their variations downstream the Lancang River in China, describes the mineralogical signatures of modern sand generated in different geological domains, and estimates sediment yield and contribution rates from different tributary catchments, distinguishing between first-cycle and recycled sediments.

2. The Lancang Basin

The Lancang River (Figure 1) originates from Mount Jifu in Zaduo County, Qinghai Province, at an elevation of 5200 m a.s.l. Within China's territory, the mainstem is 2129 km long with a drainage area of 167,487 km^2 [14]. In the headwaters, runoff ranges from 200 to 300 mm, gradually increasing as the river enters Yunnan Province. The Lancang River's annual discharge has remained relatively stable through time, although with uneven distribution during the year. Flow is concentrated between May and October and minimal in January and February [15].

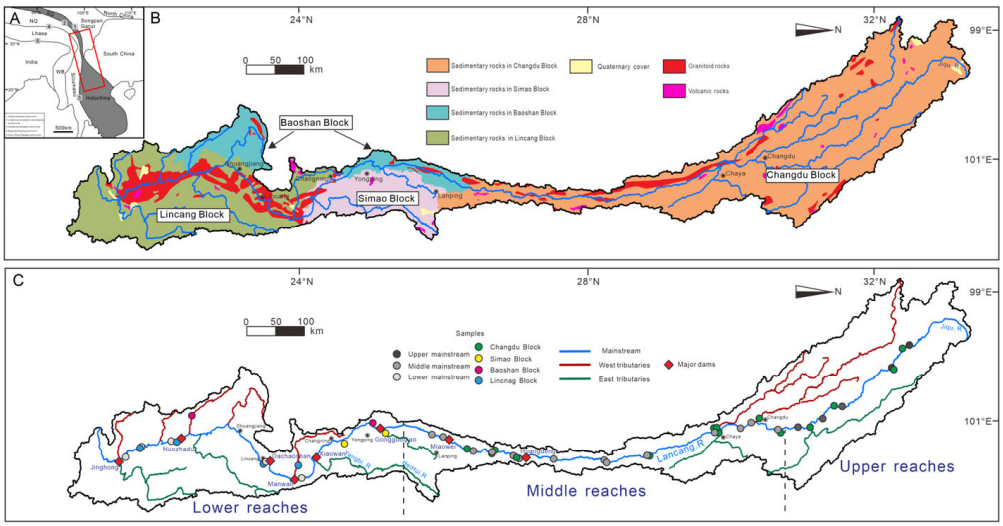

Figure 1. The Lancang River basin (**A**). (**B**) Geological map (modified from [13]). (**C**) Drainage map. Red box is Lancang River basin's position in tectonic framework.

The Lancang River (Figure 1C), flowing from the eastern margin of the Tibetan Plateau, runs nearly parallel to the Lancang suture zone [16], a region that has remained tectonically active since the late Cenozoic [17]. The river drains different geological domains (Changdu, Simao, Baoshan, and Lincang blocks [18]; Figure 1B), and its sediments thus represent a mixture of detritus shed from various sources characterized by distinct endmember compositional signatures.

2.1. Changdu Block

The Changdu block mostly consists of Triassic sedimentary rocks. Upper Paleozoic shallow marine carbonate and clastic rocks are overlain by Lower to Middle Triassic continental to transitional volcaniclastic rocks, and in turn by Upper Triassic fluvio-deltaic clastic rocks and marine limestones. Magmatic activity took place during the Triassic [19,20], and the stratigraphic succession is capped by Jurassic and Cretaceous continental red beds.

2.2. Simao Block

The Simao block is dominated by Mesozoic–Cenozoic mudrocks. Older strata, exposed on both eastern and western sides, include mainly deep-water turbidites in the east, followed by Upper Permian volcaniclastic deposits in the east. Continental to shal-

low marine feldspar-rich sandstones, mudrocks, and carbonates are overlain by Upper Carboniferous–Lower Permian volcano-sedimentary sequences in the west [21].

2.3. Baoshan Block

The Baoshan block mainly consists of Upper Paleozoic carbonates and sandstones [21–23]. Cambrian–Ordovician granites dated between 502 and 444 Ma and minor volcanic rocks dated as 499–486 Ma occur; younger granites were also intruded in Upper Paleozoic to Cenozoic strata [24–29].

2.4. Lincang Block

The Lincang block mainly consists of quartz-schists, mica-schists, and meta-granulites in the west [30–32]. Ordovician mafic-intermediate metavolcanic rocks (463–454 Ma) and granites (458.5 ± 3.0 Ma) [33–35] also occur. Devonian–Carboniferous siliciclastic strata are overlain by Permian mudrocks and limestones [21]. The Lincang plutonic belt, bracketed between the western side of the block and the Lancang mélange belt [23], mostly consists of biotite monzogranite dated as 230–200 Ma [36] and locally metamorphosed to gneiss [37,38].

3. Methods

A total of 47 sand samples were collected from active river bars in 2021 and 2023 (24 along the mainstem at 50–100 km intervals, and 23 from major tributaries). Detailed information on sampling locations and grain-size data is provided in Table 1. Grain-size analysis was conducted using a Mastersize 2000 laser particle size analyzer at the School of Geography and Ocean Sciences, Nanjing University. Grain-size parameters were calculated following Folk and Ward [39]; φ values were calculated as $\varphi = -\log_2 D$ (where D is grain size in mm).

A quartered fraction of each sample was impregnated with Araldite epoxy and cut into a standard thin section. Petrographic analyses were carried out by counting 400–500 grains per section under the microscope according to the Gazzi–Dickinson method (inherent counting error ~5% at 1σ) [40]. The classification scheme for detrital components was based on the relative proportions of the three main constituents: quartz (Q), feldspar (F), and lithic fragments (L) [41]. Polycrystalline quartz was counted as quartz; sedimentary lithics include chert and carbonate [42].

The relative sediment contributions from different tributaries and different geological units were calculated with forward mixing modeling based on petrographic data [43,44]. The forward mixing model computes compositional data (as row vectors, with columns representing variables) as non-negative linear combinations between a fixed endmember composition matrix (rows representing observations, columns representing variables) and coefficient row vectors representing the proportional contributions of each endmember to the observations [43]. We applied a filter to our data to incorporate the uncertainties of our assumptions and address the fact that natural geological complexity often diverges from theoretical models. We only used modeled compositions if the statistical distance was within 110% of the minimum value calculated using both Aitchison and Euclidean methods for each sample. Our final provenance budget and its associated uncertainties were then derived from the standard deviation of this selected set of solutions. The simulation requires first determining the endmember compositions of different tributaries and geological units, then calculating several simulated compositions by assigning different proportions of these sources [43,45]. To enhance simulation accuracy, multiple representative samples are typically averaged to better define the composition of endmember components.

Table 1. Sampling sites and grain-size parameters.

Sample ID	Downstream Distance/km	Latitude (N)	Longitude (E)	Location	River	D_{10}/φ	D_{50}/φ	D_{90}/φ	D_{mean}/φ	σ	SK
21L006	0	21.85053	101.01257	Manjucun, Jinghong	Lower Lancang River	1.736	3.028	7.117	3.647	2.053	0.513
21L007	38.8	22.01052	100.80678	Xishuangbanna Bridge	Lower Lancang River	0.069	0.803	1.773	0.831	1.042	0.342
21L008	125.9	22.50944	100.57599	Simaogang, Puer	Lower Lancang River	0.413	1.413	3.203	1.487	1.307	0.345
21L009	338.3	23.91246	100.41335	Jiezizhaicun, Yuanxian	Lower Lancang River	1.528	2.368	3.308	2.385	0.714	0.089
21L011	442.5	24.60885	100.46058	Manwan, Yunxian	Lower Lancang River	0.299	1.453	5.297	1.911	1.788	0.493
21L013	763.7	26.25866	99.1335	Dabizancun, Lanping	Middle Lancang River	1.213	2.506	7.204	3.252	2.213	0.549
21L014	793.5	26.47022	99.14607	Yingpanqiao, Laning	Middle Lancang River	2.061	4.791	8.777	5.100	2.615	0.190
21L016	872	27.07261	99.17453	Weideng, Diqing	Middle Lancang River	2.574	3.779	7.473	4.222	1.810	0.480
21L017	914.6	27.36663	99.0851	Baijixun, Diqing	Middle Lancang River	0.505	1.576	5.052	1.698	1.583	0.400
21L018	963.7	27.71149	99.04798	Yezhi, Diqing	Middle Lancang River	0.805	1.643	4.407	1.703	1.362	0.401
21L019	974.9	27.79151	99.03116	Bujiecun, Diqing	Middle Lancang River	0.295	1.118	4.042	1.182	1.428	0.417
21L020	1047.7	28.30534	98.87471	Deqin	Middle Lancang River	0.415	1.454	2.815	1.507	1.050	0.221
21L022-1	1160.8	29.09714	98.61262	Quzika, Mangkang	Middle Lancang River	0.065	1.282	2.823	1.337	1.217	0.207
21L022	1165.3	29.13235	98.63051	Lajiuxicun, Mangkang	Middle Lancang River	0.978	1.927	3.383	1.992	1.344	0.364
21L023	1232.9	29.62561	98.35249	Rumei, Mangkang	Middle Lancang River	−0.085	1.047	2.881	1.131	1.576	0.361
21L025	1386.4	30.60655	97.52622	Kagongcun, Chaya	Upper Lancang River	1.534	2.566	5.804	2.669	1.480	0.385
21L026	1433.9	30.9402	97.36719	Tigongcun, Changdu	Upper Lancang River	0.589	1.461	2.808	1.516	1.429	0.397
21L027	1461.1	31.08413	97.203	Botuocun, Changdu	Upper Lancang River	1.668	2.427	3.378	2.456	0.936	0.304
21L028	1514.4	31.46377	97.19023	Gaoatongcun, Changdu	Upper Lancang River	1.205	2.137	7.105	2.813	2.012	0.636
23L29	1561.1	31.78711	97.00243	Jiarongcun, Changdu	Upper Lancang River	1.758	3.057	5.394	3.223	1.557	0.333
23L30	1616.8	32.06843	96.76559	Bariniangcun, Nangqian	Upper Lancang River	1.541	2.133	2.789	2.143	0.490	0.062
23L31	1663.5	32.27281	96.46386	Zhangjicecun, Nangqian	Upper Lancang River	2.330	3.517	6.943	3.798	1.694	0.434

Table 1. *Cont.*

Sample ID	Downstream Distance/km	Latitude (N)	Longitude (E)	Location	River	D_{10}/φ	D_{50}/φ	D_{90}/φ	D_{mean}/φ	σ	SK
23L33	1805.2	32.84496	95.552	Duonacun, Nangqian	Upper Lancang River	2.059	2.856	4.145	2.909	1.175	0.374
23L34	1867.5	32.94123	95.138	Suijia, Zaduo	Upper Lancang River	0.828	2.051	4.998	2.316	1.751	0.430
21LB015	33.4	21.99248	100.83041	Mingjiangyuan	Liusha River	0.627	1.880	5.298	2.315	1.781	0.452
21LB013	139.1	22.57872	100.53739	Nuozhadu, Puer	Zhong River	1.081	2.254	7.800	3.422	2.593	0.651
21LB012	337.9	23.91212	100.42524	Xiushancun, Puer	Gali River	2.508	3.960	7.835	4.463	2.018	0.441
21LB011	455	24.49335	100.30111	Yunxian, Lincang	Luozha River	2.276	3.600	6.248	3.852	1.546	0.328
21LB014	197.8	22.64531	100.11734	Lancang, Puer	Hei River	2.360	3.706	6.452	3.992	1.585	0.336
21LB006	639.8	25.44094	99.28604	Wayao, Yunlong	Wayao River	0.675	2.203	4.155	2.233	1.555	0.209
21LB009	580.1	25.08667	99.75802	Yongping, Dali	Yongping River	2.804	4.315	8.367	4.902	2.139	0.452
21LB007	673	25.62547	99.35982	Yunlong	Pijiang River	2.224	3.240	7.321	3.750	1.806	0.558
21LB005	863.6	26.98093	99.21461	Biyuhexiacun, Lanping	Tongdian River	−0.059	1.212	4.476	1.609	1.953	0.477
21LB004	913.3	27.35236	99.0996	Baiji, Weixi	Yongchun River	1.171	2.240	5.380	2.542	1.588	0.460
21LB003	921.8	27.40308	99.04969	Baijixun, Weixi	Laochang River	0.362	1.688	6.861	2.683	2.448	0.580
21LB002	969.6	27.75023	99.04312	Xiacun, Weixi	Lancang River	0.680	2.045	5.648	2.230	1.758	0.365
21LB022	1389.1	30.6198	97.51119	Kagongxiang, Chaya	Sequ River	0.089	1.549	3.658	1.655	1.667	0.287
21LB023	1397.7	30.63645	97.49381	Kagongxiang	Xiqu River	0.474	5.835	9.317	5.090	3.463	−0.214
21LB026	1476.7	31.16993	97.10522	Shagongcun, Changdu	Anngqu River	1.509	2.289	3.231	2.313	0.935	0.287
21LB021	1235	29.6437	98.35329	Duibacun, Mangkang	Rongqu River	0.295	1.339	3.113	1.430	1.472	0.374
21LB024	1410.1	30.65892	97.57458	Yanduosi, Chaya	Maiqu River	1.407	3.119	8.597	4.172	2.798	0.527
21LB025	1520.1	31.50431	97.21045	Sexiongkacun, Chaya	Requ River	0.642	1.627	7.883	3.016	2.749	0.723
23LB31	1585.5	31.96893	96.94544	Gaiqu Bridge, Changdu	Ziqu River	1.499	2.342	4.986	2.405	1.345	0.397
23LB30	1597.3	32.0532	97.00347	Batongcun, Changdu	Ziqu River	1.581	2.599	6.912	2.780	1.612	0.448
23LB27	1646.4	32.14131	96.54105	Jiamashenshan, Nangqian	Qiangqu River	0.804	2.290	6.853	2.711	2.170	0.454
23LB28	1809.1	32.8746	95.57029	Duonacun, Zaduo	Shaqunqu River	1.645	2.643	6.182	3.002	1.703	0.522
23LB29	1854.5	32.89482	95.23348	Zaduo	Jinaiqu River	1.849	3.967	8.964	4.743	2.757	0.404

Note: Sample 21L006, collected at the most downstream location in the Lancang River, was designated as the 0 km reference point. The along-channel distances between 21L006 and other sampling points were calculated accordingly.

4. Results

4.1. Texture of Lancang River Sands

The studied sand samples (7 very fine, 26 fine, 13 medium, and 1 coarse; Figure 2A,B) are mainly very fine to fine in the upper reaches, medium in the middle reaches, and very fine in the lower reaches, but with great variability and no systematic downstream fining (Figure 3). The sorting coefficient ranges from 0.5 to 3.5; only 4 samples are well sorted, 30 are poorly sorted, and 14 are very poorly sorted (Figure 2C). Skewness ranges from −0.29 to 0.72; only 2 samples show negative skewness, 2 are nearly symmetrical, 6 are positively skewed, and 37 are strongly positively skewed (Figure 2D).

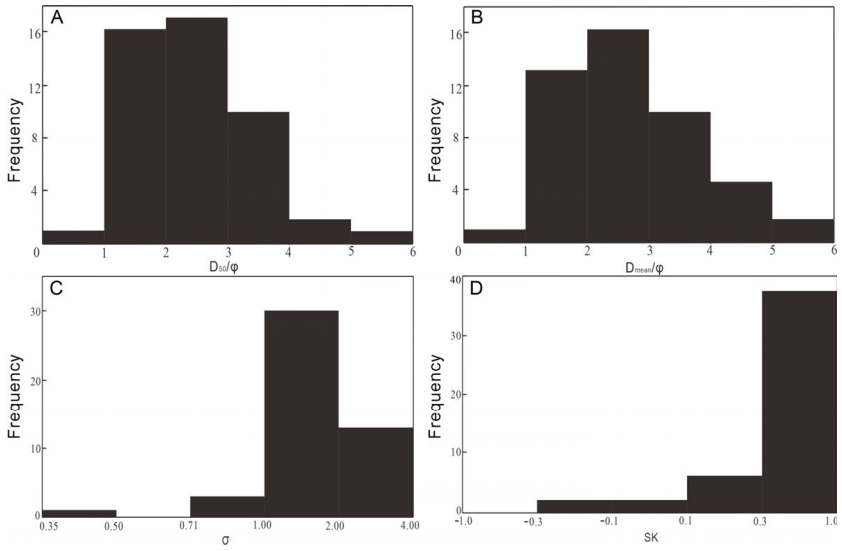

Figure 2. Frequency distribution of grain-size parameters: (**A**) D_{50}: median diameter; (**B**) D_{mean}: mean diameter; (**C**) σ: sorting coefficient; (**D**) SK: skewness.

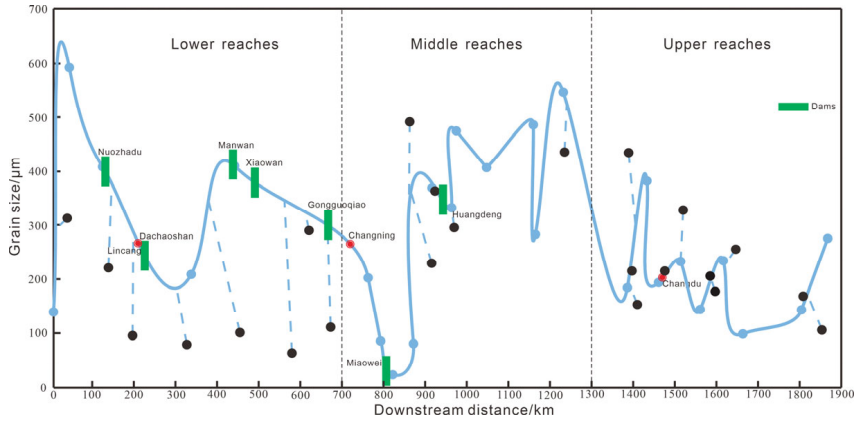

Figure 3. Variability in mean grain size of the studied sand samples along the Lancang River. Blue dots connected by value curve are mainstream samples, and black dots are tributary samples connected with dashed lines to their respective confluence points on the main stream.

Finer samples in the upper reaches have poor sorting and positive skewness, whereas coarser samples in the middle reaches have extremely positive skewness. Textural variability appears to be influenced by human impacts (e.g., hydropower stations, riverside road development, steep slope cultivations [46–50]). Natural downstream fining and selective transport make minor contributions to the grain size distribution. Eight major dams (Huangdeng, Miaowei, Gongguoqiao, Xiaowan, Manwan, Dachaoshan, Nuozhadu, and Jinghong) were built in the middle and lower reaches (Figure 1C). The proximity of

reservoir locations to the site of coarser-grain samples with extremely positive skewness suggests that cascade dams induce sediment coarsening. Because river bedload is efficiently trapped in artificial reservoirs, the enhanced erosion power of clear water downstream of dams leads to erosion and resuspension of older channel and bank deposits [51–53], explaining the coarser size and extremely positive skewness of samples collected shortly downstream of dams.

4.2. Petrography of Lancang River Sands

Lancang River sands are mostly feldspatho-quartzo-lithic (Figure 4). Quartz is mainly monocrystalline, feldspars are mostly potassic, and rock fragments are predominantly sedimentary with only minor volcanic and metamorphic types (Figure 5 and Table 2).

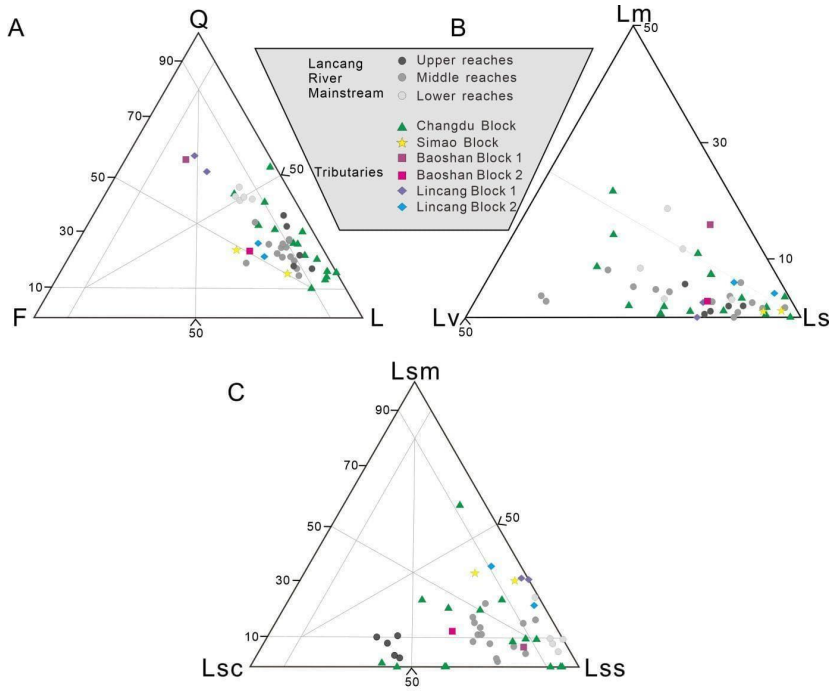

Figure 4. Sandstone petrography. (**A**) Q: quartz, F: feldspar, L: lithic plot (compositional fields after [41,42]); (**B**) Lm: metamorphic, Lv: volcanic, Ls: sedimentary lithic plot; (**C**) Lss: shale, Lsc: carbonate; Lss: sand(silt)stone lithic plot.

The Lancang mainstem is here divided into upper reaches of Changdu (5 samples), middle reaches upstream of Gongguoqiao Dam (14 samples), and lower reaches downstream (5 samples). In the upper reaches, samples are quartzo-lithic and feldspatho-quartzo-lithic (average composition $Q_{25}F_{10}L_{65}$, $Ls_{88}Lv_{10}Lm_{2}$, $Lsm_{10}Lsc_{39}Lss_{51}$). In the middle reaches, samples are mainly feldspatho-quartzo-lithic and subordinately quartzo-feldspatho-lithic and quartzo-lithic (average composition $Q_{23}F_{13}L_{64}$, $Ls_{78}Lv_{18}Lm_{4}$, $Lsm_{10}Lsc_{20}Lss_{70}$). In the lower reaches, samples are feldspatho-litho-quartzose and feldspatho-quartzo-lithic (average composition $Q_{43}F_{15}L_{42}$, $Ls_{79}Lv_{13}Lm_{8}$, $Lsm_{11}Lsc_{2}Lss_{87}$). Carbonate grains thus markedly decrease downstream, whereas quartz, feldspar, and siltstone rock fragments relatively increase.

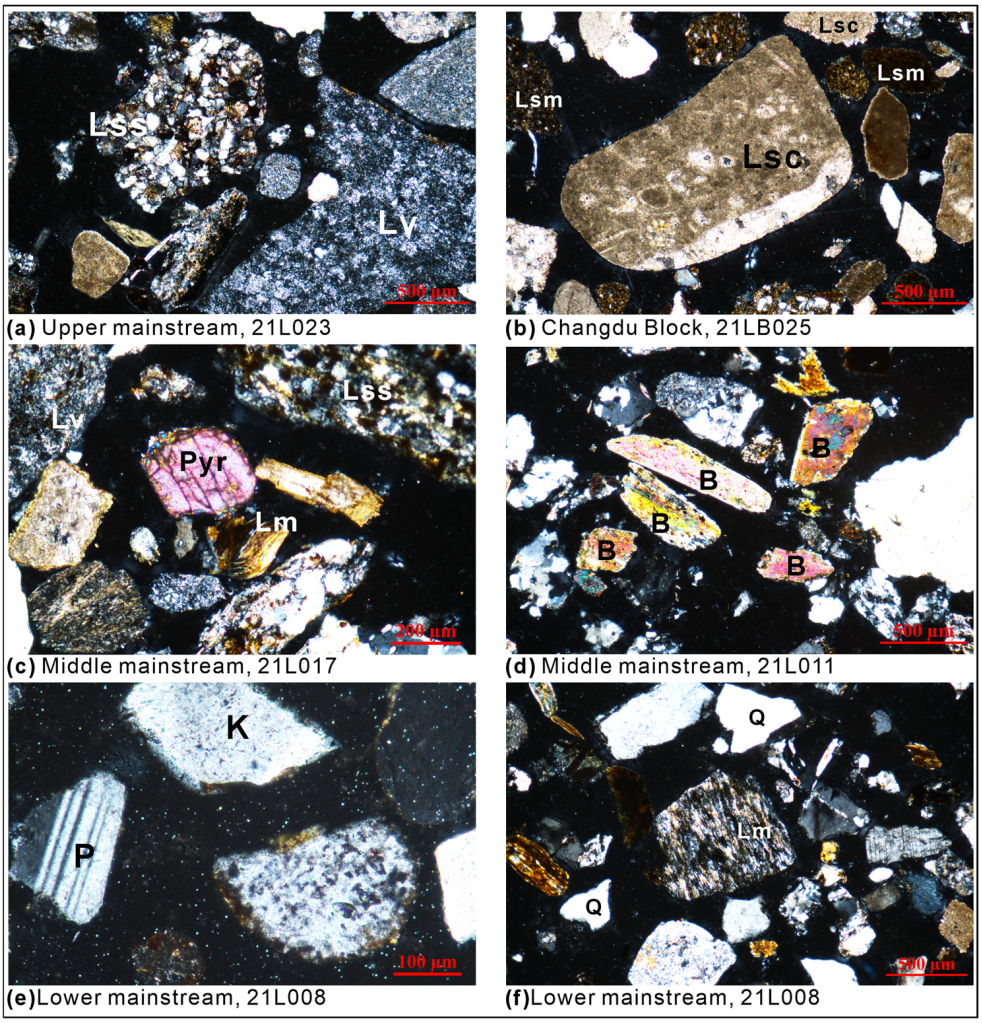

Figure 5. Petrography of Lancang River sands. Q: quartz, K: K-feldspar, P: plagioclase; L: lithics (Lv: volcanic, Lm: metamorphic, Lss: siltstone, Lsc: carbonate, Lsm: shale), B: biotite, Pyr: pyroxene.

Tributary samples are classified into four groups (Changdu, Simao, Baoshan 1 and 2, Lincang 1 and 2). The 15 tributaries draining the Changdu block (Changdu group) carry mainly quartzo-lithic and subordinately litho-quartzose, feldspatho-litho-quartzose, and feldspatho-quartzo-lithic sand (average composition $Q_{26}F_7L_{67}$, $Ls_{82}Lv_{13}Lm_5$, $Lsm_{12}Lsc_{23}Lss_{65}$). The two tributaries draining the Lanping–Simao Basin (Simao group) carry feldspatho-quartzo-lithic and quartzo-feldspatho-lithic sand (average composition $Q_{19}F_{21}L_{60}$, $Ls_{95}Lv_4Lm_1$, $Lsm_{31}Lsc_{10}Lss_{59}$). The two tributaries draining the Baoshan block carry litho-feldspatho-quartzose ($Q_{56}F_{26}L_{18}$, $Ls_{79}Lv_7Lm_{14}$, $Lsm_6Lsc_{13}Lss_{81}$; Baoshan 1 tributary) or feldspatho-quartzo-lithic sand ($Q_{23}F_{23}L_{54}$, $Ls_{85}Lv_{13}Lm_2$, $Lsm_{12}Lsc_{32}Lss_{56}$; Baoshan 2 tributary). Tributaries draining the Lincang block carry litho-feldspatho-quartzose (average composition $Q_{54}F_{21}L_{25}$, $Ls_{84}Lv_{14}Lm_2$, $Lsm_{31}Lsc_1Lss_{68}$; Lincang 1 tributaries mainly draining the Lincang plutonic belt) or feldspatho-litho-quartzose sand (average composition $Q_{24}F_{19}L_{57}$, $Ls_{91}Lv_4Lm_5$, $Lsm_{28}Lsc_6Lss_{66}$; Lincang 2 tributary).

Table 2. Petrographic composition of Lancang River sand (grain counts).

Sample ID	Drainage Area	Q	F	L	Lsm	Lsc	Lss	Cht	Lv	Lm	HM	Total
21L006	Lower Mainstem	158	57	164	30	2	93	0	20	19	21	400
21L007	Lower Mainstem	180	58	155	11	0	105	5	29	5	7	400
21L008	Lower Mainstem	156	64	160	14	5	122	0	14	5	22	402
21L009	Lower Mainstem	163	67	153	9	4	97	0	30	13	17	400
21L011	Lower Mainstem	131	41	144	2	1	99	0	15	27	84	400
21L013	Middle Mainstem	91	59	254	28	59	159	0	4	4	6	410
21L014	Middle Mainstem	76	42	266	43	59	147	0	13	4	22	406
21L016	Middle Mainstem	70	94	201	29	9	139	0	12	12	35	400
21L017	Middle Mainstem	82	43	259	12	29	133	0	64	21	16	400
21L018	Middle Mainstem	106	33	247	38	30	104	7	55	13	14	400
21L019	Middle Mainstem	66	44	276	10	30	174	2	48	12	14	400
21L020	Middle Mainstem	105	34	250	3	45	139	3	48	12	11	400
21L022-1	Middle Mainstem	97	49	247	4	35	108	0	91	9	7	400
21L022	Middle Mainstem	100	61	228	17	54	123	1	27	6	11	400
21L023	Middle Mainstem	97	43	252	12	35	104	2	92	7	8	400
21L025	Upper Mainstem	103	45	247	34	21	168	3	15	6	5	400
21L026	Upper Mainstem	59	48	288	29	65	165	0	29	0	5	400
21L027	Upper Mainstem	129	62	194	23	39	106	2	17	7	15	400
21L028	Upper Mainstem	85	55	256	35	55	138	3	23	2	4	400
23L29	Upper Mainstem	122	27	229	7	99	77	0	33	13	23	401
23L30	Upper Mainstem	146	25	234	6	106	88	0	33	1	7	412
23L31	Upper Mainstem	86	33	272	20	133	93	0	21	5	14	405
23L33	Upper Mainstem	72	47	274	25	136	81	0	27	5	8	401
23L34	Upper Mainstem	69	27	300	28	128	102	0	39	3	5	401
21LB015	Lincang Block	153	61	83	21	0	47	2	13	0	103	400
21LB013	Lincang Block	102	73	217	66	17	105	1	15	13	8	400
21LB012	Lincang Block	79	70	219	44	6	156	0	4	9	32	400
21LB011	Lincang Block	170	67	63	16	1	35	1	8	2	132	432
21LB014	Baoshan Block	126	58	43	2	4	25	3	3	6	180	407
21LB006	Baoshan Block	79	78	184	19	50	86	1	23	5	59	400
21LB009	Simao Block	58	59	266	84	39	134	0	6	3	17	400
21LB007	Simao Block	93	105	197	55	8	120	2	10	2	5	400
21LB005	Changdu Block	128	60	192	15	17	120	0	19	21	21	401
21LB004	Changdu Block	78	13	289	0	11	177	0	60	41	22	402
21LB003	Changdu Block	62	9	309	0	19	183	0	80	27	26	406
21LB002	Changdu Block	56	14	320	0	13	183	0	55	69	11	401
21LB022	Changdu Block	116	41	216	17	14	143	5	21	16	27	400
21LB023	Changdu Block	59	0	341	67	67	201	0	6	0	0	400
21LB026	Changdu Block	170	67	153	26	37	63	11	11	5	10	400
21LB021	Changdu Block	163	37	200	15	26	125	0	32	2	3	403
21LB024	Changdu Block	102	26	267	59	29	162	2	14	1	5	400
21LB025	Changdu Block	87	25	283	60	92	104	10	12	5	5	400
23LB31	Changdu Block	105	31	263	0	81	126	0	51	5	13	412
23LB30	Changdu Block	116	12	256	0	72	116	0	63	5	16	400
23LB27	Changdu Block	52	17	317	3	148	99	0	65	2	21	407
23LB28	Changdu Block	202	6	173	0	84	68	0	19	2	19	400
23LB29	Changdu Block	40	40	310	166	23	105	3	2	11	10	400

Qm: monocrystalline quartz, Qp: polycrystalline quartz, Pl: plagioclase, Kf: K-feldspar, L: lithic fragments (Lsm: shale, Lsc: carbonate, Lss: siltstone, Cht: chert, Lv: volcanic, Lm: metamorphic), HM: heavy minerals.

Quartz is prevalent and siltstone lithics least abundant in Baoshan 1 and Lincang 1 tributaries, feldspar least abundant in Changdu tributaries, and volcanic and carbonate grains more common in Changdu and Baoshan 2 tributaries. Compositional variability along the Lancang mainstem is illustrated in Figure 6.

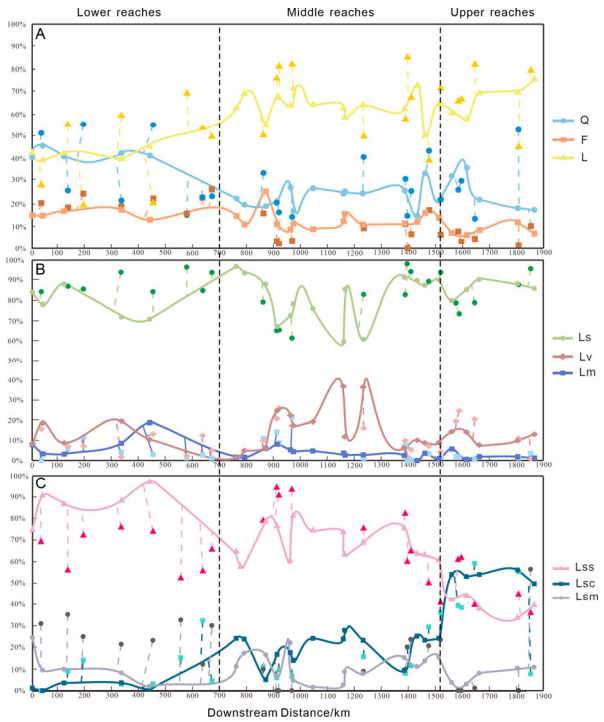

Figure 6. Compositional variability along the Lancang mainstem. (**A**) QFL percentages, (**B**) lithic fragments percentages, (**C**) sedimentary rock fragments percentages. Q: quartz, F: feldspar, L: lithics (Lm: metamorphic, Lv: volcanic, Ls: sedimentary; Lss: shale, Lsc: carbonate, Lss: siltstone). Mainstem samples are connected with a smooth curve, tributary samples with dashed lines to their respective confluences with the mainstem.

5. Discussion

5.1. Provenance Budget Based on Petrographic Data

Forward mixing calculations indicate that final Lancang sand upstream of the China border originates mainly from the Lincang block (52 ± 20%; 6 ± 6% for Lincang 1 and 46 ± 15% for Lincang 2), subordinately from the Baoshan block (32 ± 9%; 2 ± 2% for Baoshan1 and 30 ± 9% for Baoshan 2), and in minor part from the Changdu and Simao blocks (8 ± 7% each) (Figure 7).

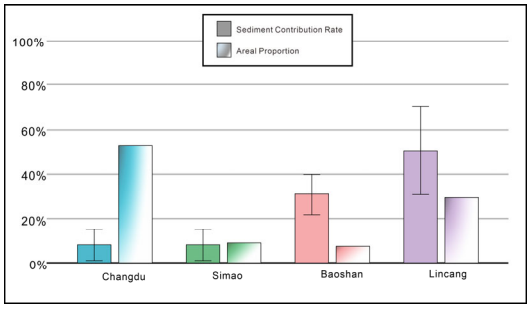

Figure 7. Sediment yields from different geological units in the Lancang catchment.

Sand is calculated to be overwhelmingly (92 ± 8%) recycled from sedimentary rocks drained by Changdu, Simao, Baoshan 2, and Lincang 2 tributaries, whereas first-cycle contribution from granitic sources drained by Lincang1 and Baoshan 1 tributaries is assessed to be only 8 ± 8%. Taking into account the basin areas occupied by the Changdu (85,335 km^2, 53% of total area), Simao (15,660 km^2, 10%), Baoshan (13,546 km^2, 8%), and Lincang blocks (45,549 km^2, 28%), the highest sediment yields are assessed for the Baoshan and Lincang blocks (Figure 7). Sediment supply results are higher for tributaries in the upper reaches

than for tributaries in the middle reaches, rising again for tributaries in the lower reaches (Figure 7).

Our estimates differ from previous indications based on U-Pb zircon dating and geochemical research, suggesting that Lancang River sand mainly originates from the Northern Qiangtang block [11,12]. To check for this discrepancy, we analyzed the available hydrological data from five gauging stations (data shown in Supplementary Materials Table S1). The recorded average annual discharges and sediment loads are 30.0 km^3 and 22.7 $\times$ 10^6 t for the Gongguoqiao station, 37.1 km^3 and 42.5 $\times$ 10^6 t for the Gajiu station, 28.2 km^3 and 22.7 $\times$ 10^6 t for the Jiuzhou station, 22.8 km^3 and 22.7 $\times$ 10^6 t for the Liutongjiang station, and 56.8 km^3 and 82.5 $\times$ 10^6 t for the Yunxianghong station. Based on these data, 22.7 $\times$ 10^6 t, 0.004 $\times$ 10^6 t, 19.2 $\times$ 10^6 t, and 40.1 $\times$ 10^6 t of sediment are produced in the four river tracts delimited by dams, with corresponding annual sediment yields of 295 t/km^2, 0.2 t/km^2, 1097 t/km^2, and 1173 t/km^2 (Figure 8). The resulting higher sediment yields from the lower reaches are consistent with the outcome of forward mixing calculations.

Figure 8. Sediment yield in four tracts of the Lancang catchment based on hydrological data (data from hydrological yearbook of Sanjiang catchment from 1958 to 1987 (Table S1)). River course in blue.

5.2. First-Cycle Versus Recycled River Sand

Sedimentary rocks are the primary source of Lancang River sediments. This is testified by the abundance of shale, siltstone, sandstone, and carbonate rock fragments in most samples (e.g., 21LB006, 21LB012, and 21LB013), whereas only a few (e.g., 21LB011, 21LB014, and 21LB015) contain a significant amount of first-cycle detritus, including minor igneous and metamorphic rock fragments and more biotite and heavy minerals. Most Lancang River sand is thus recycled. Regarding optical characteristics, first-cycle samples exhibit quartz and feldspar grains with clear boundaries and smooth surfaces. In recycled samples, quartz grains are instead commonly well-rounded and show turbid surfaces and concave outlines, and feldspars appear notably altered. All samples are, however, mixed, largely first-cycle samples also containing some sedimentary rock fragments and largely recycled samples including volcanic or plutonic grains as well as hornblende, pyroxene, and epidote.

5.3. Durability of Carbonate Grains

Carbonate rock fragments (mostly sparry to bioclastic limestone) are most abundant in the upper reaches (Figure 4), where they represent 50–60% of sedimentary rock fragments (Figure 6C). This proportion decreases to 10–30% in the middle reaches, where carbonate particles are mostly micritic limestone with minor sparite locally containing quartz-rich silt, and becomes very low in the lower reaches, where mainly micritic lithics occur. Such a

downstream decrease in carbonate grains primarily reflects provenance, carbonate rocks being mostly extensively exposed in the Changdu block. The presence of large reservoirs prevents the transportation of these grains downstream, where carbonate exposures are sparse. However, cathodoluminescence analysis could help distinguish different types of carbonate fragments and assess their degree of abrasion and roundness, providing valuable insights into source lithologies and transport pathways [54,55].

In large rivers draining humid regions and characterized by high discharge and waters with high pCO_2 levels, such as the Brahmaputra, the Congo, or the Pearl River, carbonate grains may be efficiently dissolved [56–61]. Selective mechanical breakdown of carbonate grains may also occur (Figure 4 in [59]). These effects are, however, difficult to separate from the effect of downstream dilution by carbonate-poor tributary sands, enhanced in highly man-regulated river systems by efficient sediment sequestration in reservoirs upstream. The natural controls of compositional change between different downstream tracts of the heavily dam-segmented course of the Lancang River are consequently hard to evaluate.

6. Conclusions

Sands carried by the Lancang (Upper Mekong) River are mainly feldspatho-quartzo-lithic with dominant sedimentary rock fragments. Quartz content increases downstream at the expense of lithic fragments. Carbonate rock fragments decrease markedly, whereas siltstone/sandstone fragments relatively increase. Sand is thus mostly recycled from sedimentary rocks, with minor contributions from igneous rocks. Based on forward modeling calculations, sand is mostly derived from the Lancang (52 ± 20%) and Baoshan blocks (32 ± 9%), with minor contributions from the Simao and Changdu blocks (~8% each).

Most textural and compositional variability along the Lancang River was mainly induced by anthropogenic impact. Eight major dams were built in the middle and lower reaches, leading to extreme segmentation of sediment fluxes and thus preventing us from separately identifying and evaluating the effect of natural processes, such as the potential selective chemical or physical breakdown of more labile grains, including carbonate and shale rock fragments. To evaluate erosion rates, we thus resorted to the analysis of the available hydrological data from five gauging stations, which allowed us to constrain provenance budgets and calculate annual sediment yields increasing from ~300 t/km^2 in the upper reaches to >1000 t/km^2 in the lower reaches.

Supplementary Materials: The following supporting information can be downloaded at https://www.mdpi.com/article/10.3390/geosciences15110415/s1, Table S1: Multiyear flow table and annual sediment transport.

Author Contributions: Conceptualization, X.H.; methodology, X.H.; validation, D.F., X.H. and W.L.; formal analysis, D.F., X.H., W.L. and F.C.; investigation, D.F. and X.H.; resources, X.H. and D.F.; data curation, D.F. and X.H.; writing—original draft, D.F., X.H., and E.G.; visualization, X.H. and D.F.; Supervision, X.H.; project administration, X.H. All authors have read and agreed to the published version of the manuscript.

Funding: This research was financially supported by the Second Tibetan Plateau Scientific Expedition Research Program (STEP, Grant No. 2019QZKK020402) and GeoX' Interdisciplinary Project of Frontiers Science Center for Critical Earth Material Cycling, Grant No. 20250102.

Data Availability Statement: The original contributions presented in this study are included in the article/Supplementary Materials. Further inquiries can be directed to the corresponding authors.

Acknowledgments: The authors are grateful to Wendong Liang, Xiaolong Dong, and Keran Li for their assistance with sample collection and express their sincere gratitude to the editors and the anonymous reviewers for their valuable comments and suggestions.

Conflicts of Interest: The authors declare no conflicts of interest.

Glossary

Block	Tectono-stratigraphic terranes accreted to an orogenic belt and characterized by a unique assemblage of lithologies, stratigraphic succession, and tectonic evolution.
First-cycle sediment	Sediment typically enriched in feldspars, volcanic and/or metamorphic rock fragments, and heavy minerals derived directly from igneous rocks and/or metamorphic basement.
Recycled sediment	Sediment typically enriched in durable minerals (quartz, zircon, tourmaline, rutile) derived from the erosion of pre-existing lithified sedimentary rocks or loose siliciclastic deposits.

References

1. Burbank, D.W.; Blythe, A.E.; Putkonen, J.; Pratt-Sitaula, B.; Gabet, E.; Oskin, M.; Barros, A.; Ojha, T.P. Decoupling of erosion and precipitation in the Himalayas. *Nature* **2003**, *426*, 652–655. [CrossRef] [PubMed]
2. Godard, V.; Bourlès, D.L.; Spinabella, F.; Burbank, D.W.; Bookhagen, B.; Fisher, G.B.; Moulin, A.; Léanni, L. Dominance of tectonics over climate in Himalayan denudation. *Geology* **2014**, *42*, 243–246. [CrossRef]
3. Wang, P.; Scherler, D.; Liu-Zeng, J.; Mey, J.; Avouac, J.-P.; Zhang, Y.; Shi, D. Tectonic control of Yarlung Tsangpo Gorge revealed by a buried canyon in Southern Tibet. *Science* **2014**, *346*, 978–981. [CrossRef] [PubMed]
4. Sickmann, Z.T.; Chheda, T.D.; Capaldi, T.N.; Thomson, K.D.; Paull, C.K.; Graham, S.A. Using provenance analysis in an Anthropocene natural laboratory. *Quat. Sci. Rev.* **2019**, *221*, 105890. [CrossRef]
5. Liang, W.; Hu, X. Research progress of sand composition in river sediments. *Acta Geol. Sin.* **2023**, *97*, 2975–2991. [CrossRef]
6. Harris, N. The elevation history of the Tibetan Plateau and its implications for the Asian monsoon. *Palaeogeogr. Palaeoclimatol. Palaeoecol.* **2006**, *241*, 4–15. [CrossRef]
7. Kapp, P.; Murphy, M.A.; Yin, A.; Harrison, T.M.; Ding, L.; Guo, J. Mesozoic and Cenozoic tectonic evolution of the Shiquanhe area of western Tibet. *Tectonics* **2003**, *22*, 1029. [CrossRef]
8. Walling, D.E. Chapter 6—The Sediment Load of the Mekong River. In *The Mekong*; Campbell, I.C., Ed.; Academic Press: Cambridge, MA, USA, 2009; pp. 113–142. [CrossRef]
9. Zhang, J.; Yang, H.; Liu-Zeng, J.; Ge, Y.; Wang, W.; Yao, W.; Xu, S. Reconstructing the incision of the Lancang River (Upper Mekong) in southeastern Tibet below its prominent knickzone using fluvial terraces and transient tributary profiles. *Geomorphology* **2021**, *376*, 107551. [CrossRef]
10. Liu, Z.; Colin, C.; Trentesaux, A.; Siani, G.; Frank, N.; Blamart, D.; Farid, S. Late Quaternary climatic control on erosion and weathering in the eastern Tibetan Plateau and the Mekong Basin. *Quat. Res.* **2005**, *63*, 316–328. [CrossRef]
11. Zhang, P.; Najman, Y.; Mei, L.; Millar, I.; Sobel, E.R.; Carter, A.; Barfod, D.; Dhuime, B.; Garzanti, E.; Govin, G.; et al. Palaeodrainage evolution of the large rivers of East Asia, and Himalayan-Tibet tectonics. *Earth-Sci. Rev.* **2019**, *192*, 601–630. [CrossRef]
12. Chen, X.; Chen, Y.; Bao, C.; Li, G.; Yan, J.; Li, D. U-Pb dating and Hf isotopic composition of detrital zircons in the sediments from the Lancang River and its geological significance. *Geoscience* **2014**, *28*, 1170–1182.
13. Huyan, Y.; Zhang, B.; Wang, X.; Lu, Y.; Liu, F. Geochemistry of the Lancang River (Upper Mekong River) overbank sediments: Implications for provenance, weathering and sedimentary characteristics. *Appl. Geochem.* **2023**, *156*, 105747. [CrossRef]
14. Chen, Q.; Kong, X. *Lancang-Mekong River Basin Basic Data Collections*; Yunnan Science and Technical Press: Kunming, China, 2000; pp. 1–259.
15. Li, L.; Li, H.; Wang, J. Analysis on hydrological and water quality character and their spatial and temporal distribution in Lancang River. *Sci. Geogr. Sin.* **2002**, *22*, 49–56.
16. Zhang, P.Z.; Shen, Z.; Wang, M.; Gan, W.; Bürgmann, R.; Molnar, P.; Wang, Q.; Niu, Z.; Sun, J.; Wu, J.; et al. Continuous deformation of the Tibetan Plateau from global positioning system data. *Geology* **2004**, *32*, 809–812. [CrossRef]
17. Deng, J.; Wang, Q.; Li, G.; Santosh, M. Cenozoic tectono-magmatic and metallogenic processes in the Sanjiang region, southwestern China. *Earth-Sci. Rev.* **2014**, *138*, 268–299. [CrossRef]
18. Liu, Z.; Colin, C.; Huang, W.; Le, K.P.; Tong, S.; Chen, Z.; Trentesaux, A. Climatic and tectonic controls on weathering in south China and Indochina Peninsula: Clay mineralogical and geochemical investigations from the Pearl, Red, and Mekong drainage basins. *Geochem. Geophys. Geosyst.* **2007**, *8*, Q05005. [CrossRef]
19. Xia, D. *Lithostratigraphy of Xizang Autonomous Region*; China University of Geosciences Press: Wuhan, China, 1997; pp. 1–302.
20. Wang, L. *Geological Map and Instruction Manual of the Qinghai Tibet Plateau and Its Adjacent Areas*; Geology Press: Beijing, China, 2013; pp. 1–155.

21. Zhong, D. *The Paleo-Tethys Orogenic Belt in Western Sichuan and Yunnan Province*; Science Press: Beijing, China, 1998; pp. 1–242.
22. Metcalfe, I. Gondwana dispersion and Asian accretion: Tectonic and palaeogeographic evolution of eastern Tethys. *J. Asian Earth Sci.* **2013**, *66*, 1–33. [CrossRef]
23. Metcalfe, I. Multiple Tethyan ocean basins and orogenic belts in Asia. *Gondwana Res.* **2021**, *100*, 87–130. [CrossRef]
24. Lin, Y.; Wei, G.; Zengtao, C.; Yulong, Y.; Yan, T. LA-ICP-MS Zircon U-Pb Geochronology and Petrology of the Muchang Alkali Granite, Zhenkang County, Western Yunnan Province, China. *Acta Geol. Sin. Engl. Ed.* **2010**, *84*, 1488–1499. [CrossRef]
25. Dong, M.; Dong, G.; Mo, X.; Santosh, M.; Zhu, D.; Yu, J.; Nie, F.; Hu, Z. Geochemistry, zircon U–Pb geochronology and Hf isotopes of granites in the Baoshan Block, Western Yunnan: Implications for Early Paleozoic evolution along the Gondwana margin. *Lithos* **2013**, *179*, 36–47. [CrossRef]
26. Li, D.; Chen, Y.; Hou, K.; Luo, Z. Origin and evolution of the Tengchong block, southeastern margin of the Tibetan Plateau: Zircon U–Pb and Lu–Hf isotopic evidence from the (meta-) sedimentary rocks and intrusions. *Tectonophysics* **2016**, *687*, 245–256. [CrossRef]
27. Zhu, R.; Lai, S.; Qin, J.; Zhao, S.; Santosh, M. Strongly peraluminous fractionated S-type granites in the Baoshan Block, SW China: Implications for two-stage melting of fertile continental materials following the closure of Bangong-Nujiang Tethys. *Lithos* **2018**, *316–317*, 178–198. [CrossRef]
28. Huan, Y.; Li, X.; Lei, H. Zircon U-Pb age and geochemical characteristics of the early palaeozoic granite in Shiganhe-Pinghe area, west Yunnan. *Miner. Resour. Geol.* **2017**, *31*, 150–157.
29. Tao, Y.; Zhu, F.; Ma, Y.; Ye, L.; Cheng, Z. La-ICP-MS analysis of granite in Benzhishan aera, Baoshan Block. *Acta Mineral. Sin.* **2009**, *29*, 329.
30. Liu, B.; Peng, T.; Fan, W.; Zhao, G.; Gao, J.; Dong, X.; Peng, B. Tectonic Evolution and Paleoposition of the Baoshan and Lincang Blocks of West Yunnan During the Paleozoic. *Tectonics* **2020**, *39*, e2019TC006028. [CrossRef]
31. Liu, G. Petrology Component and Geochronology of Early Paleozoic Proto-Tethys Ophiolite Mélange in SW Yunnan. Ph.D. Thesis, China University of Geosciences, Wuhan, China, 2020; pp. 1–153.
32. Zhao, T.Y. Early Paleozoic Proto-Tethys Tectonics Evolution in SW Yunnan: Constraints from Detrital Zircon U-Pb Geochronology and Granite Associations. Ph.D. Thesis, China University of Geosciences, Wuhan, China, 2019; pp. 1–133.
33. Nie, X.; Feng, Q.; Qian, X.; Wang, Y. Magmatic Record of Prototethyan Evolution in SW Yunnan, China: Geochemical, Zircon U–Pb Geochronological and Lu–Hf Isotopic Evidence from the Huimin Metavolcanic Rocks in the Southern Lancangjiang Zone. *Gondwana Res.* **2015**, *28*, 757–768. [CrossRef]
34. Xing, X.; Wang, Y.; Cawood, P.A.; Zhang, Y. Early Paleozoic accretionary orogenesis along northern margin of Gondwana constrained by high-Mg metaigneous rocks, SW Yunnan. *Int. J. Earth Sci.* **2017**, *106*, 1469–1486. [CrossRef]
35. Zhao, T.; Feng, Q.; Metcalfe, I.; Milan, L.A.; Liu, G.; Zhang, Z. Detrital zircon U-Pb-Hf isotopes and provenance of Late Neoproterozoic and Early Paleozoic sediments of the Simao and Baoshan blocks, SW China: Implications for Proto-Tethys and Paleo-Tethys evolution and Gondwana reconstruction. *Gondwana Res.* **2017**, *51*, 193–208. [CrossRef]
36. Dong, G.; Mo, X.; Zhao, Z.; Zhu, D.; Goodman, R.C.; Kong, H.; Wang, S. Zircon U–Pb dating and the petrological and geochemical constraints on Lincang granite in Western Yunnan, China: Implications for the closure of the Paleo-Tethys Ocean. *J. Asian Earth Sci.* **2013**, *62*, 282–294. [CrossRef]
37. Luo, B. Petrology Geochemistry, Chronology Characteristics and Their Significances of Early Paleozoic Granite in Yunxian, West Yunnan. Master's Thesis, Chengdu University of Technology, Chengdu, China, 2020; pp. 1–60.
38. Peng, Z.; Zhang, J.; Guan, J.; Zhang, Z.; Han, W.; Fu, Y. The discovery of early-midde ordovician granitic gneiss from the giant Lincang batholith in Sangjiang area of western Yunnan and its geological implications. *Earth Sci.* **2018**, *43*, 2571–2585.
39. Ingersoll, R.V.; Bullard, T.F.; Ford, R.L.; Grimm, J.P.; Pickle, J.D.; Sares, S.W. The effect of grain size on detrital modes: A test of the Gazzi-Dickinson point-counting method. *J. Sediment. Res.* **1984**, *54*, 103–116. [CrossRef]
40. Folk, R.L.; Ward, W.C. Brazos River bar [Texas]; A study in the significance of grain size parameters. *J. Sediment. Res.* **1957**, *27*, 3–26. [CrossRef]
41. Garzanti, E. From static to dynamic provenance analysis—Sedimentary petrology upgraded. *Sediment. Geol.* **2016**, *336*, 3–13. [CrossRef]
42. Garzanti, E. Petrographic classification of sand and sandstone. *Earth-Sci. Rev.* **2019**, *192*, 545–563. [CrossRef]
43. Weltje, G.J. End-member modeling of compositional data: Numerical-statistical algorithms for solving the explicit mixing problem. *Math. Geol.* **1997**, *29*, 503–549. [CrossRef]
44. Resentini, A.; Goren, L.; Castelltort, S.; Garzanti, E. Partitioning sediment flux by provenance and tracing erosion patterns in Taiwan. *J. Geophys. Res. Earth Surf.* **2017**, *122*, 1430–1454. [CrossRef]
45. Liang, W.; Garzanti, E.; Hu, X.; Resentini, A.; Vezzoli, G.; Yao, W. Tracing erosion patterns in South Tibet: Balancing sediment supply to the Yarlung Tsangpo from the Himalaya versus Lhasa Block. *Basin Res.* **2022**, *34*, 411–439. [CrossRef]
46. Fu, K.; Yang, W.; Su, B.; Li, D.; Li, M.; Zhang, J.; Song, J. Response of river sediments to basin environmental changes: A case study of the Lancang River. *Prog. Geogr.* **2015**, *34*, 1148–1155.

47. Mo, B. Application of Particle Size Analysis in Sedimentary Characteristics: A case study of quaternart sediments from Zhujiang delta. *Nei Jiang Ke Ji* **2018**, *39*, 24–25.
48. Syvitski, J.P.M.; Vörösmarty, C.J.; Kettner, A.J.; Green, P. Impact of Humans on the Flux of Terrestrial Sediment to the Global Coastal Ocean. *Science* **2005**, *308*, 376–380. [CrossRef]
49. Dai, S.; Yang, S.; Li, M. The sharp decrease in suspended sediment supply from China's rivers to the sea: Anthropogenic and natural causes. *Hydrol. Sci. J.* **2009**, *54*, 135–146. [CrossRef]
50. Wang, H.; Sun, F. Variability of annual sediment load and runoff in the Yellow River for the last 100 years (1919–2018). *Sci. Total Environ.* **2021**, *758*, 143715. [CrossRef] [PubMed]
51. Grant, G.E. The Geomorphic Response of Gravel-Bed Rivers to Dams: Perspectives and Prospects. In *Gravel-Bed Rivers*; John Wiley & Sons, Inc.: Hoboken, NJ, USA, 2012; pp. 165–181. [CrossRef]
52. Topping, D.J.; Rubin, D.M.; Melis, T.S. Coupled changes in sand grain size and sand transport driven by changes in the upstream supply of sand in the Colorado River: Relative importance of changes in bed-sand grain size and bed-sand area. *Sediment. Geol.* **2007**, *202*, 538–561. [CrossRef]
53. Guo, X.; Zhu, X.; Yang, Z.; Ma, J.; Xiao, S.; Ji, D.; Liu, D. Impacts of cascade reservoirs on the longitudinal variability of fine sediment characteristics: A case study of the Lancang and Nu Rivers. *J. Hydrol.* **2020**, *581*, 124343. [CrossRef]
54. Pszonka, J.; Wendorff, M. Cathodoluminescence-revealed diagenesis of carbonates and feldspars in Cergowa sandstones (Oligocene), Outer Carpathians. *Gospod. Surowcami Miner.* **2014**, *30*, 21–36.
55. Pszonka, J.; Wendorff, M. Carbonate cements and grains in submarine fan sandstones—The Cergowa Beds (Oligocene, Carpathians of Poland) recorded by cathodoluminescence. *Int. J. Earth Sci.* **2017**, *106*, 269–282. [CrossRef]
56. Singh, S.K.; France-Lanord, C. Tracing the distribution of erosion in the Brahmaputra watershed from isotopic compositions of stream sediments. Earth Planet. *Sci. Lett.* **2002**, *202*, 645–662.
57. Garzanti, E.; Vermeesch, P.; Vezzoli, G.; And'o, S.; Botti, E.; Limonta, M.; Dinis, P.; Hahn, A.; Baudet, D.; De Grave, J.; et al. Congo River sand and the equatorial quartz factory. *Earth-Sci. Rev.* **2019**, *197*, 102918. [CrossRef]
58. Garzanti, E.; He, J.; Barbarano, M.; Resentini, A.; Li, C.; Yang, L.; Yang, S.; Wang, H. Provenance versus weathering control on sediment composition in tropical monsoonal climate (South China)-2. Sand petrology and heavy minerals. *Chem. Geol.* **2021**, *564*, 119997.
59. Garzanti, E. The maturity myth in sedimentology and provenance analysis. *J. Sediment. Res.* **2017**, *87*, 353–365. [CrossRef]
60. Xu, Y.; Jin, Z.; Gou, L.F.; Galy, A.; Jin, C.; Chen, C.; Li, C.; Deng, L. Carbonate weathering dominates magnesium isotopes in large rivers: Clues from the Yangtze River. *Chem. Geol.* **2022**, *588*, 120677. [CrossRef]
61. Li, C.; Wang, S.; Bai, X.; Tan, Q.; Li, H.; Li, Q.; Deng, Y.; Yang, Y.; Tian, S.; Hu, Y. Estimation of carbonate rock weathering-related carbon sink in global major river basins. *Acta Geogr. Sin.* **2019**, *74*, 1319–1332.